Grading Glial Tumors with Amide Proton Transfer MR Imaging: Different Analytical Approaches

Article type: Clinical Study

Akihiko Sakata, MD[1], Tomohisa Okada, MD, PhD[1*], Akira Yamamoto, MD, PhD[1], Mitsunori Kanagaki, MD, PhD[1], Yasutaka Fushimi, MD, PhD[1], Tsutomu Okada MD, PhD[1], Toshiki Dodo, MD[1], Yoshiki Arakawa, MD, PhD[2], Benjamin Schmitt PhD[3], Susumu Miyamoto, MD, PhD[2], Kaori Togashi, MD, PhD[1]

[1]Department of Diagnostic Imaging and Nuclear Medicine, [2]Department of Neurosurgery, Kyoto University Graduate School of Medicine, Kyoto, 606-8507 Japan.

[3]Healthcare Sector, Imaging & Therapy Division, Magnetic Resonance, Siemens AG, 91052 Erlangen, Germany.

*Corresponding Author: Tomohisa Okada, MD, PhD

Department of Diagnostic Imaging and Nuclear Medicine, Kyoto University Graduate School of Medicine. 54 Shogoin Kawahara-cho, Sakyo-ku, Kyoto, 606-8507, Japan.

Phone: +81-75-751-3760, FAX: +81-75-771-9709

E-mail: tomokada@kuhp.kyoto-u.ac.jp

Contact address of all authors:

Akihiko Sakata, Tomohisa Okada, Akira Yamamoto, Mitsunori Kanagaki, Yasutaka Fushimi, Tsutomu Okada, Toshiki Dodo, Kaori Togashi.

Department of Diagnostic Imaging and Nuclear Medicine, Kyoto University Graduate School of Medicine, Kyoto, 54 Shogoin Kawahara-cho, Sakyo-ku, Kyoto, 606-8507, Japan.

Yoshiki Arakawa, Susumu Miyamoto

Department of Neurosurgery Kyoto University Graduate School of Medicine, 54 Shogoin Kawahara-cho, Sakyo-ku, Kyoto, 606-8507, Japan.

Benjamin Schmitt PhD

Siemens Ltd, Healthcare Sector, Melbourne, Australia

Grading Glial Tumors with Amide Proton Transfer MR Imaging: Different Analytical Approaches

Article type: Clinical Study

Abstract

Amide proton transfer (APT) magnetic resonance (MR) imaging is gaining attention for its capability for grading glial tumors. Usually, a representative slice is analyzed. Different definitions of tumor areas have been employed in previous studies. We hypothesized that the accuracy of APT imaging for brain tumor grading may depend upon the analytical methodology used, such as selection of regions of interest (ROIs), single or multiple tumor slices, and whether or not there is normalization to the contralateral white matter. This study was approved by the institutional review board, and written informed consent was waived. Twenty-six patients with histologically proven glial tumors underwent preoperative APT imaging with a three-dimensional gradient-echo sequence. Two neuroradiologists independently analyzed APT asymmetry (APTasym) images by placing ROIs on both a single representative slice (RS) and all slices including tumor (i.e. whole tumor: WT). ROIs indicating tumor extent were separately defined on both FLAIR and, if applicable, contrast-enhanced T1-weighted images (CE-T1WI), yielding four mean APTasym values (RS-FLAIR, WT-FLAIR, RS-CE-T1WI, and WT-CE-T1WI). The maximum values were also measured using small ROIs, and their differences among grades were evaluated. Receiver operating characteristic (ROC) curve analysis was also conducted on mean and maximum values. Intra-class correlation coefficients for inter-observer agreement were excellent. Significant differences were observed between high- and low-grade gliomas for all five methods ($P < 0.01$). ROC curve analysis found no statistically significant difference among them. This study clarifies that single-slice APT analysis is

robust despite tumor heterogeneity, and can grade glial tumors with or without the use of contrast material.

Keywords

Magnetic resonance imaging; Amide proton transfer imaging; Chemical exchange saturation transfer;

Glioma grading

Introduction

Amide proton transfer (APT) magnetic resonance (MR) imaging is a subtype of chemical exchange saturation transfer (CEST) imaging that uses a sensitivity enhancement mechanism to indirectly detect hydrogen outside of free water molecules [1-4]. APT imaging has recently been introduced into clinical practice and is capable of visualizing endogenous proteins and peptides through saturation of the amide protons in the peptide bonds [5-7]. APT imaging signal is measured as a reduction of bulk water intensity by chemical exchange with magnetically labeled amide protons at +3.5 ppm (APT frequency), which is compared with those at the control frequency (−3.5 ppm) and calculated as APT asymmetry (APTasym) values.

APTasym values provide information on amide concentration and tissue physicochemical properties (pH and temperature) that influence the relative proton exchange rate. Clinical applications of APT imaging have been investigated in a wide variety of pathologies [8-11] including brain tumors [6, 12-17]. Previous reports have demonstrated that APT imaging is useful in delineation of high-grade glioma, determination of histological grades, and detection of recurrence [17].

Although APT scanning is technically feasible using currently available clinical MR imaging systems, other methodological issues still need to be addressed. One of the most relevant is establishing which part of the tumor should be measured to generate APTasym values. For example, given the heterogeneity of brain tumor tissue [18-21], different values would be derived if measurements were

taken from different areas within the same tumor [22]. Furthermore, earlier analyses quantified APTasym values derived from a single representative slice [6, 12-14, 17], without examining all the slices containing the tumor. Techniques to delineate tumors, including T2-weighted images (T2WI), FLAIR, and contrast-enhanced (CE) T1-weighted images (T1WI); and handling of derived values (mean or maximum values), as well as their normalization [17], have been variously employed.

The purpose of this study was to investigate differences in the accuracy of APTasym mean and maximum values derived from areas defined on a single representative slice and defined by examination of all tumor-containing slices using FLAIR and contrast-enhanced T1WI for grading gliomas, with and without normalization.

Material and Methods

MR scans including APT imaging were conducted in patients after written informed consent. We conducted a retrospective analysis of these studies, which was approved by the institutional review board. Written informed consent was waived.

Patients

Thirty-three consecutive patients with a postoperative diagnosis of supratentorial glioma between December 2012 and February 2014 were included. Exclusion criteria were: 1) surgical intervention or chemo-radiation therapy prior to imaging, 2) recurrent cases, 3) age under 18 years, and 4) severe image

artifacts caused by motion or susceptibility artifact from dental work. Seven cases were excluded for these reasons. A total of 26 patients (19 were male and 7 were female; mean age 59.1 years, range 21–90 years) were enrolled in this study. The pathological diagnosis was made by surgical resection (n = 22) or stereotactic biopsy (n = 4). Pathological diagnoses were made according to WHO classification (2007) [23]. Immunohistochemical staining for IDH1-R132H was conducted using an antibody specific for the mutant IDH1-R132H protein (Dianova GmbH, Hamburg, Germany) in all but 2 patients with insufficient material [24].

MR Imaging Scan

MR imaging was conducted using a 3 T MR imaging scanner (MAGNETOM Trio, a Tim System®: Siemens Healthcare, Erlangen, Germany) with a 32-channel head coil. APT imaging was performed using a three-dimensional, gradient-echo pulse sequence [9, 25, 26] with the following settings: time of repetition [TR]/time of echo [TE], 8.3/3.3 ms; flip angle [FA], 12°; resolution, 1.72 × 1.72 × 4 mm; 24 slices. Pre-saturation pulses consisted of three consecutive RF pulses of 100-ms duration with 100-ms inter-pulse delays and 2μT time-average amplitude. Image sets were acquired without pre-saturation pulse (S0 image) and with pre-saturation pulses at different offset frequencies $\Delta\omega$ (0, ± 0.6, ± 1.2, ± 1.8, ± 2.4, ± 3.0, ± 3.6, ± 4.2, and ± 4.8 ppm) from the bulk water resonance. Total scan time was 5 minutes 31 seconds.

APT effect was calculated as the asymmetry of the magnetization transfer rate (MTRasym) with the following equation: APTasym = (S[−3.5 ppm] − S[+3.5 ppm])/S0 × 100%. The APTasym at +3.5 ppm was obtained after linear interpolation between the originally sampled points to a resolution of 0.1 ppm and subsequent correction for inhomogeneity of the static magnetic field by Z-spectrum shifting, as previously described [26]. This method has also been successfully applied to the glycosaminoglycan CEST, which requires smaller frequency shift compared with APT, with 3T clinical MRI scanner [25].

FLAIR images were acquired with the following parameters: TR/TE, 12000/100 ms; time of inversion, 2760 ms; FA, 120°; resolution, 0.69 × 0.69 × 4 mm; 35 slices. To cover the whole brain, pre-contrast and CE T1WI were acquired using magnetization-prepared rapid-acquisition gradient echo with the following settings: TR/TE, 6/2.26 ms; FA, 15°; resolution, 0.9 × 0.9 × 0.9 mm. Contrast materials used were 0.1 mmol/kg of gadopentetate dimeglumine (Magnevist®, Bayer, Osaka, Japan) or gadoteridol (ProHance®; Eisai, Tokyo, Japan).

Image Processing and Analysis

Images were co-registered with SPM8® software (Wellcome Trust Centre for Neuroimaging, London, UK) implemented on Matlab® (The MathWorks, Inc., Natick MA, USA) using a previously described method [27]. S0 images, APTasym images, and post-contrast T1WI were co-registered to FLAIR images and re-sliced. Registration was visually inspected and manually corrected, if necessary. Images were

analyzed using regions of interest (ROIs) on software (Image J ver. 1.48; NIH, Bethesda, MD, USA). Two neuroradiologists (A.S. and T.D., both with 6 years of experience in neuroradiology), who were blinded to the patient's clinical information, analyzed the images independently.

Different methods were used for defining tumor extent: FLAIR or contrast-enhanced T1WI on a representative single-slice (RS) or on all slices containing the tumor (i.e. whole-tumor: WT), resulting in four different ROI definitions: RS-FLAIR, RS-CE-T1WI, WT-FLAIR, and WT-CET1WI for average APTasym values. For single-slice analysis, a representative slice including the largest solid portion of the tumor was selected. ROIs were drawn around abnormal signal areas on FLAIR images. In the cases of tumors with an enhancing portion, the ROIs were drawn around the enhancing area (assumed to be viable tumor core) on the CE-T1WI (Fig. 1) [12-16]. For maximum APTasym (MAX) values, four circular ROIs of more than 25 pixels were carefully placed in the solid component of a tumor to include the area with the highest APTasym values determined with visual inspection on a representative slice, and the four maximum values were averaged, resulting in the MAX value (Fig. 2) [17]. The APTasym signal was also measured in a larger circular ROI placed around normal-appearing white matter (NAWM) for normalization. Normalized APTasym values were calculated as APTasym tumor − APTasym NAWM [17].

Vessels, hemorrhage, and necrotic foci were carefully avoided when placing ROIs [17]. All ROIs were superimposed on the APTasym images, and areas affected by susceptibility artifacts were

excluded. In total, the following five measurements were used for analysis: RS-FLAIR, WT-FLAIR, RS-CE-T1WI, WT-CE-T1WI and MAX.

Statistical Analysis

Agreement of the two evaluators in measuring the tumor APTasym values was calculated as the intra-class correlation coefficient (ICC) for each of the five different analysis methods. The values of the two evaluators were averaged.

APTasym and normalized APTasym values were compared between high- and low-grade tumors using a two-sample t-test, as well as among the tumor grades using analysis of variance (ANOVA) with the Tukey–Kramer post hoc test. Receiver operating characteristic (ROC) curve analysis was conducted for the five measurement methods, and areas under the curve (AUCs) were statistically compared using a method by Delong et al [28]. A P value < 0.05 was considered statistically significant. All statistical analyses were performed with MedCalc ver.12.5.0.0 (MedCalc Software®, Mariakerke, Belgium).

Results

Pathological Diagnosis

Eighteen of the 26 patients had pathologically confirmed high-grade glioma (glioblastoma, Grade 4: 12;

anaplastic astrocytoma, Grade 3: three; and anaplastic oligoastrocytoma, Grade 3: three). The other eight patients were diagnosed as low-grade gliomas (diffuse astrocytoma, Grade 2: five; oligodendroglioma, Grade 2: two; and oligoastrocytoma, Grade 2: one). Six of the 26 patients had glioma with oligocytic component. Positive finding of immunohistochemistiry of IDH1-R132H was observed in 8 (33%) cases.

APTasym measurements of the brain tumors

For all five measurement methods, ICCs were 0.92–0.99 and considered excellent (Table 1). Mean APTasym values and normalized APTasym values derived with the five methods are summarized in Table 2 and 3.

Table 2 shows mean APTasym of high-and low-grade glioma obtained by five different ROI settings. In APTasym with or without normalization, significant differences were found between high- and low-grade gliomas using all five measurement methods ($P < 0.01$, two-sample t test, Table 2). In APTasym analysis without normalization, RS-CE-T1WI, RS-FLAIR, and WT-CE-T1WI showed significant differences between Grades 2 and 4, and Grades 3 and 4, but not between Grades 2 and 3. WT-FLAIR and MAX found significant differences between Grades 2 and 4 only. Normalized APTasym showed significant differences between Grades 2 and 4, and Grades 3 and 4, but not between Grades 2 and 3 on RS-CE-T1WI and WT-CE-T1WI. Significant differences were found only between Grades 2

and 4 on RS-FLAIR, WT-FLAIR, and MAX images (Table 3).

ROC analysis

In differentiation of glioma grades, AUCs were 0.81–0.88 for the five measurement methods with a sensitivity of 66.7–83.3 % and a specificity of 75.0–100 % (Fig. 3 and Table 4). Although WT-FLAIR and MAX showed slightly lower grading capability than the three other measurement methods with or without normalization, no statistically significant difference was found among them. A representative case is presented in Fig. 4.

Discussion

To the best of our knowledge, this is the first comprehensive study of APTasym analysis methodologies for glioma grading. The results show that APTasym analysis based on a single representative slice has high accuracy in grading diffuse glioma, comparable to whole tumor analysis. Additionally, APTasym analysis can be performed without contrast material, using FLAIR images.

Accurate grading of gliomas is of utmost importance, because the therapeutic approach and prognosis differ considerably. Contrast-enhanced T1WI shows disruption of the blood-brain barrier, which is frequently associated with high-grade tumor. However, contrast material enhancement alone is not always accurate in predicting tumor grade. Other MR imaging techniques, such as diffusion weighted

image (DWI) or MR spectroscopy (MRS) are also used for characterization of brain tumors [29, 30]. These methods have frequently shown conflicting results or overlap in measured values among different grades [31, 32]. Therefore, an imaging method that complements other MR methods and improves accuracy in grading gliomas promises to be useful.

APT imaging is an emerging molecular MR method based on the CEST mechanism of exchangeable amide protons. Previous studies have successfully shown that APT imaging is useful in providing physiologic information on gliomas in a mouse model [6, 22, 33, 34] and in human patients [12-17]. APT imaging can differentiate radiation necrosis from glioblastoma recurrence [33], and shows treatment effect [22, 34] prior to visible size decrease [22]. However, analytical methods in previous studies have varied, and the optimal method had not been clarified. Common to all of the previous studies is the analysis of a single representative slice [12-17], mainly because a single slice is acquired to reduce scan time.

It is well known that brain tumors, especially high-grade gliomas, are characterized by marked tissue heterogeneity, i.e., hyper- and hypocellularity, necrosis, hemorrhage, and vascular proliferation, as well as heterogeneous gene expression [21], as seen in other malignancies [35]. Recently, Vargas et al. [36] showed a significant association between pathological grades and enhancement of renal cell carcinoma, when the entire tumor was measured; however, no association was found when measurement was assessed on a single representative slice. This raised the question of the appropriateness of single-

slice APTasym measurement.

In this study, no significant difference in staging accuracy was observed between high- and low-grade gliomas among five different measurement methodologies employing ROC analysis. Mean APTasym values for different tumor grades were nearly equivalent among WT-CE-T1WI, RS-CE-T1WI, and RS-FLAIR, which also shared similar cut-off values. This suggests that, despite intra-tumoral heterogeneity, APTasym analysis of a representative slice is sufficient for differentiation of tumor grades.

Delineation of tumor extent is an important issue. A conservative definition is to include contrast-enhancing areas for glioblastoma. However, usually no contrast enhancement is observed in low-grade gliomas and in some cases of Grade 3 tumors. Zhou et al. placed ROIs over the solid portions of tumors based on contrast-enhanced T1WI, while abnormal signal intensity on T2WI/FLAIR was used when no contrast enhancement was observed [13, 16]. This method may cause some bias for upstaging in high-grade gliomas. Jones et al. [12] and Togao et al. [17] used circular ROIs over high APTasym areas in the tumor, referencing conventional MR images. This method is advantageous for depicting malignant traits, which would potentially be underscored when mean values in a large ROI are used [12, 17]. For all these different analytical approaches, this study has clarified excellent inter-rater reproducibility. We also showed that there is no significant difference in grading accuracy among them. APT imaging seems to relatively unaffected by probable intra-tumoral tissue heterogeneity or variabilities in ROI placement.

ROI placement on FLAIR abnormalities is simple, and may reduce of the need for contrast

material administration, which is beneficial for follow-up examinations, especially in patients with renal insufficiency. It is well known that high-intensity foci on FLAIR images are considered to signify both tumor infiltration and peri-tumoral edema [19]. The former is located near the tumor core, whereas the latter is at the periphery. WT-FLAIR analysis included the complete peripheral abnormal signal area that was likely mainly edema, and resulted in lowering the mean APTasym values of high-grade gliomas. The RS-FLAIR method should be used, because it had virtually the same grading accuracy as RS-CE-T1WI and WT-CE-T1WI, as shown by the AUC values.

It should also be noted that the APTasym can be affected by many factors [5]. To eliminate the effect of native MTRasym, presumably caused by the solid-phase magnetization transfer effect and possible intra-molecular and inter-molecular nuclear Overhauser effects of aliphatic protons [37], the magnitude of APTasym is often determined from the difference between MTRasym at the lesion and the contralateral NAWM in previous brain studies [17, 22], and normalized APTasym values were derived. However, we found no obvious difference in grading accuracy with or without normalization, which is in line with a previous study [17], owing probably to the stability of APTasym values in NAWM.

Three-dimensional acquisition has advantages in that it can cover a whole tumor, but it requires a longer acquisition time, up to 10 min, with a turbo-spin-echo sequence [15]. Even the gradient-echo acquisition used in this study took approximately 6 min to include the entire cerebrum. Such a long acquisition can result in motion artifacts that degrade APT images and impose a heavy burden on the

patient. These problems are easily mitigated with two-dimensional acquisition, whose capability has been proven comparable to that of a three-dimensional scan in this study. In addition to diffusion-weighted imaging and MR spectroscopy, APT imaging may provide a diagnostic adjunct for grading gliomas.

There are some limitations to our study. First, the patient population was relatively small, but the number of included patients was second only to one previous study [17]. Further investigation that includes a larger population is warranted to strengthen the statistical power. Second, our study included biopsy cases. There is the possibility of histopathological misdiagnosis attributable to sampling error in the pathological examination because of the histologic heterogeneity of tumor tissues. Finally, we did not compare other noninvasive techniques such as DWI or MRS in diagnostic capability, which is another area to be investigated.

In conclusion, single-representative slice, APT imaging analysis differentiated between low- and high-grade gliomas with equivalent accuracy to APT whole tumor analysis. The reasonable scan time of single-slice acquisition facilitates the use of two-dimensional APT imaging. Combined with FLAIR images, the need for contrast enhancement might also be reduced.

Acknowledgments

The authors express their sincere gratitude to Mr. Katsutoshi Murata, Siemens Japan, KK for his assistance in optimization of APT imaging in this study.

Ethical standards

This study complies with the current laws of the country in which they were performed.

Conflict of interest

Benjamin Schmitt is an employee of Siemens AG. The other authors have no conflicts of interest related to this study.

References

1. Ward KM, Balaban RS (2000) Determination of pH using water protons and chemical exchange dependent saturation transfer (CEST). Magn Reson Med 44: 799-802

2. Ward KM, Aletras AH, Balaban RS (2000) A new class of contrast agents for MRI based on proton chemical exchange dependent saturation transfer (CEST). J Magn Reson 143: 79-87 doi:10.1006/jmre.1999.1956

3. Sherry AD, Woods M (2008) Chemical exchange saturation transfer contrast agents for magnetic resonance imaging. Annu Rev Biomed Eng 10: 391-411 doi:10.1146/annurev.bioeng.9.060906.151929

4. van Zijl PC, Yadav NN (2011) Chemical exchange saturation transfer (CEST): what

is in a name and what isn't? Magn Reson Med 65: 927-948 doi:10.1002/mrm.22761

5. Zhou J, Payen JF, Wilson DA, Traystman RJ, van Zijl PC (2003) Using the amide proton signals of intracellular proteins and peptides to detect pH effects in MRI. Nat Med 9: 1085-1090 doi:10.1038/nm907

6. Zhou J, Lal B, Wilson DA, Laterra J, van Zijl PC (2003) Amide proton transfer (APT) contrast for imaging of brain tumors. Magn Reson Med 50: 1120-1126 doi:10.1002/mrm.10651

7. Zhou J, Yan K, Zhu H (2012) A simple model for understanding the origin of the amide proton transfer MRI signal in tissue. Appl Magn Reson 42: 393-402 doi:10.1007/s00723-011-0306-5

8. Sun PZ, Benner T, Copen WA, Sorensen AG (2010) Early experience of translating pH-weighted MRI to image human subjects at 3 Tesla. Stroke 41: S147-151 doi:10.1161/STROKEAHA.110.595777

9. Gerigk L, Schmitt B, Stieltjes B, Roder F, Essig M, Bock M, Schlemmer HP, Rothke M (2012) 7 Tesla imaging of cerebral radiation necrosis after arteriovenous malformations treatment using amide proton transfer (APT) imaging. J Magn Reson Imaging 35: 1207-1209 doi:10.1002/jmri.23534

10. Jia G, Abaza R, Williams JD, Zynger DL, Zhou J, Shah ZK, Patel M, Sammet S,

Wei L, Bahnson RR, Knopp MV (2011) Amide proton transfer MR imaging of prostate cancer: a preliminary study. J Magn Reson Imaging 33: 647-654 doi:10.1002/jmri.22480

11. Dula AN, Arlinghaus LR, Dortch RD, Dewey BE, Whisenant JG, Ayers GD, Yankeelov TE, Smith SA (2013) Amide proton transfer imaging of the breast at 3 T: Establishing reproducibility and possible feasibility assessing chemotherapy response. Magn Reson Med 70: 216-224 doi:10.1002/mrm.24450

12. Jones CK, Schlosser MJ, van Zijl PC, Pomper MG, Golay X, Zhou J (2006) Amide proton transfer imaging of human brain tumors at 3T. Magn Reson Med 56: 585-592 doi:10.1002/mrm.20989

13. Zhou J, Blakeley JO, Hua J, Kim M, Laterra J, Pomper MG, van Zijl PC (2008) Practical data acquisition method for human brain tumor amide proton transfer (APT) imaging. Magn Reson Med 60: 842-849 doi:10.1002/mrm.21712

14. Wen Z, Hu S, Huang F, Wang X, Guo L, Quan X, Wang S, Zhou J (2010) MR imaging of high-grade brain tumors using endogenous protein and peptide-based contrast. Neuroimage 51: 616-622 doi:10.1016/j.neuroimage.2010.02.050

15. Zhao X, Wen Z, Zhang G, Huang F, Lu S, Wang X, Hu S, Chen M, Zhou J (2013) Three-dimensional turbo-spin-echo amide proton transfer MR imaging at 3-Tesla and its application to high-grade human brain tumors. Mol Imaging Biol 15: 114-122

doi:10.1007/s11307-012-0563-1

16. Zhou J, Zhu H, Lim M, Blair L, Quinones-Hinojosa A, Messina SA, Eberhart CG, Pomper MG, Laterra J, Barker PB, van Zijl PC, Blakeley JO (2013) Three-dimensional amide proton transfer MR imaging of gliomas: Initial experience and comparison with gadolinium enhancement. J Magn Reson Imaging doi:10.1002/jmri.24067

17. Togao O, Yoshiura T, Keupp J, Hiwatashi A, Yamashita K, Kikuchi K, Suzuki Y, Suzuki SO, Iwaki T, Hata N, Mizoguchi M, Yoshimoto K, Sagiyama K, Takahashi M, Honda H (2014) Amide proton transfer imaging of adult diffuse gliomas: correlation with histopathological grades. Neuro Oncol 16: 441-448 doi:10.1093/neuonc/not158

18. Earnest Ft, Kelly PJ, Scheithauer BW, Kall BA, Cascino TL, Ehman RL, Forbes GS, Axley PL (1988) Cerebral astrocytomas: histopathologic correlation of MR and CT contrast enhancement with stereotactic biopsy. Radiology 166: 823-827 doi:10.1148/radiology.166.3.2829270

19. Tovi M, Hartman M, Lilja A, Ericsson A (1994) MR imaging in cerebral gliomas. Tissue component analysis in correlation with histopathology of whole-brain specimens. Acta Radiol 35: 495-505

20. Hobbs SK, Shi G, Homer R, Harsh G, Atlas SW, Bednarski MD (2003) Magnetic resonance image-guided proteomics of human glioblastoma multiforme. J Magn Reson

Imaging 18: 530-536 doi:10.1002/jmri.10395

21. Sottoriva A, Spiteri I, Piccirillo SG, Touloumis A, Collins VP, Marioni JC, Curtis C, Watts C, Tavare S (2013) Intratumor heterogeneity in human glioblastoma reflects cancer evolutionary dynamics. Proc Natl Acad Sci U S A 110: 4009-4014 doi:10.1073/pnas.1219747110

22. Sagiyama K, Mashimo T, Togao O, Vemireddy V, Hatanpaa KJ, Maher EA, Mickey BE, Pan E, Sherry AD, Bachoo RM, Takahashi M (2014) In vivo chemical exchange saturation transfer imaging allows early detection of a therapeutic response in glioblastoma. Proc Natl Acad Sci U S A doi:10.1073/pnas.1323855111

23. Kleihues P LD, Wiestler OD, Burger PC, Scheithauer BW (2007) WHO grading of tumours of the central nervous system. In: Louis DN, Ohgaki H, Wiestler OD, Cavenee WK, (ed) WHO classification of tumours of the central nervous system. 4th edn. IARC, Lyon, pp. 10-11.

24. Agarwal S, Sharma MC, Jha P, Pathak P, Suri V, Sarkar C, Chosdol K, Suri A, Kale SS, Mahapatra AK (2013) Comparative study of IDH1 mutations in gliomas by immunohistochemistry and DNA sequencing. Neuro Oncol 15: 718-726 doi:10.1093/neuonc/not015

25. Schmitt B, Zaiss M, Zhou J, Bachert P (2011) Optimization of pulse train

presaturation for CEST imaging in clinical scanners. Magn Reson Med 65: 1620-1629 doi:10.1002/mrm.22750

26. Schmitt B, Zbyn S, Stelzeneder D, Jellus V, Paul D, Lauer L, Bachert P, Trattnig S (2011) Cartilage quality assessment by using glycosaminoglycan chemical exchange saturation transfer and (23)Na MR imaging at 7 T. Radiology 260: 257-264 doi:10.1148/radiol.11101841

27. Palumbo B, Angotti F, Marano GD (2009) Relationship between PET-FDG and MRI apparent diffusion coefficients in brain tumors. Q J Nucl Med Mol Imaging 53: 17-22

28. DeLong ER, DeLong DM, Clarke-Pearson DL (1988) Comparing the areas under two or more correlated receiver operating characteristic curves: a nonparametric approach. Biometrics 44: 837-845

29. Cha S (2006) Update on brain tumor imaging: from anatomy to physiology. AJNR Am J Neuroradiol 27: 475-487

30. Essig M, Anzalone N, Combs SE, Dorfler A, Lee SK, Picozzi P, Rovira A, Weller M, Law M (2012) MR imaging of neoplastic central nervous system lesions: review and recommendations for current practice. AJNR Am J Neuroradiol 33: 803-817 doi:10.3174/ajnr.A2640

31. Sugahara T, Korogi Y, Kochi M, Ikushima I, Shigematu Y, Hirai T, Okuda T, Liang

L, Ge Y, Komohara Y, Ushio Y, Takahashi M (1999) Usefulness of diffusion-weighted MRI with echo-planar technique in the evaluation of cellularity in gliomas. J Magn Reson Imaging 9: 53-60

32. Lam WW, Poon WS, Metreweli C (2002) Diffusion MR imaging in glioma: does it have any role in the pre-operation determination of grading of glioma? Clin Radiol 57: 219-225 doi:10.1053/crad.2001.0741

33. Zhou J, Tryggestad E, Wen Z, Lal B, Zhou T, Grossman R, Wang S, Yan K, Fu DX, Ford E, Tyler B, Blakeley J, Laterra J, van Zijl PC (2011) Differentiation between glioma and radiation necrosis using molecular magnetic resonance imaging of endogenous proteins and peptides. Nat Med 17: 130-134 doi:10.1038/nm.2268

34. Hong X, Liu L, Wang M, Ding K, Fan Y, Ma B, Lal B, Tyler B, Mangraviti A, Wang S, Wong J, Laterra J, Zhou J (2014) Quantitative multiparametric MRI assessment of glioma response to radiotherapy in a rat model. Neuro Oncol 16: 856-867 doi: 10.1093/neuonc/not245

35. Gerlinger M, Rowan AJ, Horswell S, Larkin J, Endesfelder D, Gronroos E, Martinez P, Matthews N, Stewart A, Tarpey P, Varela I, Phillimore B, Begum S, McDonald NQ, Butler A, Jones D, Raine K, Latimer C, Santos CR, Nohadani M, Eklund AC, Spencer-Dene B, Clark G, Pickering L, Stamp G, Gore M, Szallasi Z, Downward J, Futreal PA, Swanton C

(2012) Intratumor heterogeneity and branched evolution revealed by multiregion sequencing. N Engl J Med 366: 883-892 doi:10.1056/NEJMoa1113205

36. Vargas HA, Delaney HG, Delappe EM, Wang Y, Zheng J, Moskowitz CS, Tan Y, Zhao B, Schwartz LH, Hricak H, Russo P, Akin O (2013) Multiphasic contrast-enhanced MRI: single-slice versus volumetric quantification of tumor enhancement for the assessment of renal clear-cell carcinoma fuhrman grade. J Magn Reson Imaging 37: 1160-1167 doi:10.1002/jmri.23899

37. Paech D, Zaiss M, Meissner JE, Windschuh J, Wiestler B, Bachert P, Neumann JO, Kickingereder P, Schlemmer HP, Wick W, Nagel AM, Heiland S, Ladd ME, Bendszus M, Radbruch A (2014) Nuclear overhauser enhancement mediated chemical exchange saturation transfer imaging at 7 Tesla in glioblastoma patients. PLoS One 9: e104181 doi:10.1371/journal.pone.0104181

Figure legends

Fig. 1 A representative case of a 72-year-old man with glioblastoma (Grade 4) on FLAIR (a), contrast-enhanced T1-weighted images (b) and co-registered APTasym image (c). ROIs were drawn based on abnormal high signal intensity on FLAIR (red mask, d) and contrast-enhanced T1-weighted images (blue mask, e). Then, these two ROIs were superimposed on co-registered APTasym images (f).

Fig. 2 ROI measurements were conducted for maximum of the APTasym images with reference to contrast-enhanced T1 weighted images (a) so that cystic change, hemorrhage and necrotic component are not included. Four circular ROIs were carefully placed within the contrast-enhanced areas to include the area with the highest APT signal (b) determined by visual inspection.

Fig. 3 ROC analysis of APTasym values in differentiating high- and low-grade gliomas (a) with or (b) without normalization (n = normalized value). AUCs were 0.81–0.88 for the five measurement methods irrespective of normalization. The ROC analysis showed no statistically significant difference in grading accuracy among RS-FLAIR, WT-FLAIR, RS-CE-T1WI, WT-CE-T1WI, and MAX.

ROC: Receiver operating curve, RS: Representative-slice, WT: Whole-tumor, CE: Contrast-enhanced, T1WI: T1-weighted images, MAX: Maximum.

Fig. 4 Slice differences in APTasym imaging of a 77-year-old man with glioblastoma. FLAIR images (a–d) show a large tumor mainly located in the right frontal lobe. Contrast-enhanced T1-weighted images (e–h) show a heterogeneously enhancing tumor with large areas of necrosis. In this lesion, APTasym images (i–l) show hyperintensity in all four slices with a similar degree of heterogeneity.

Fig. 1

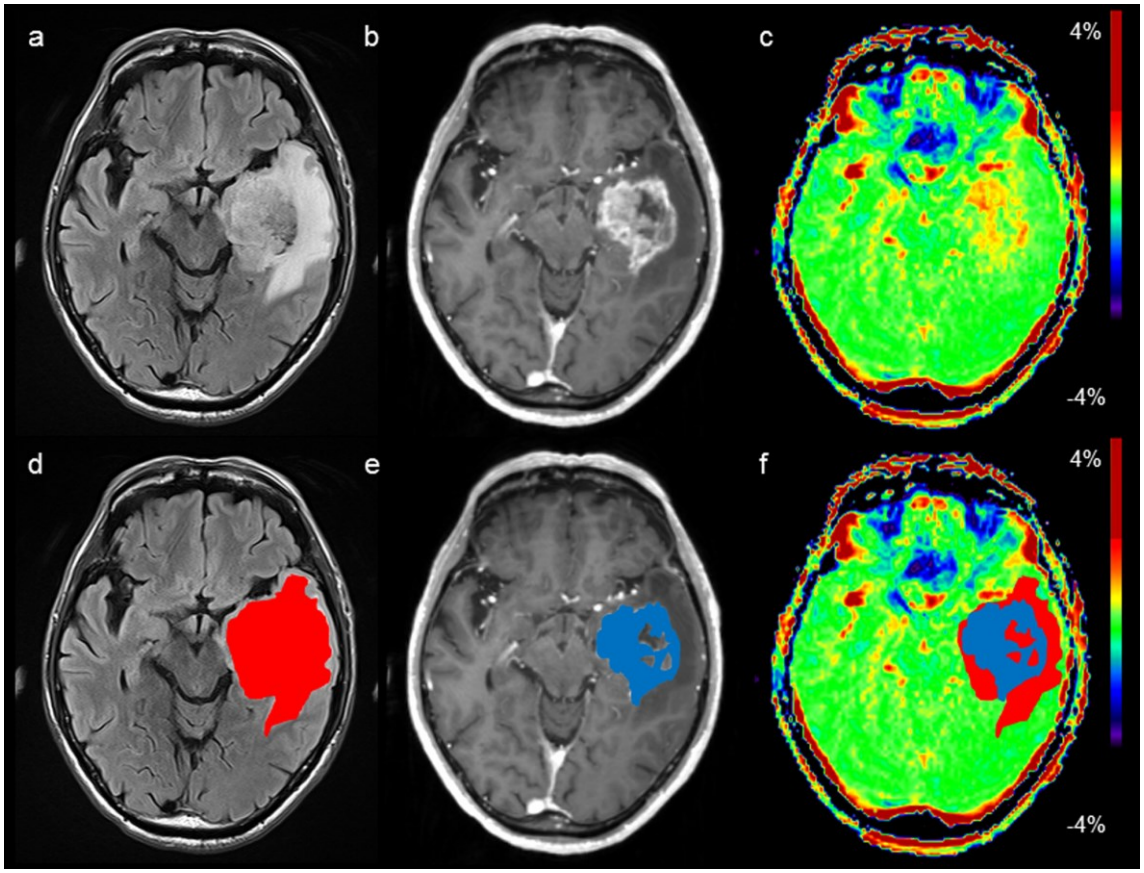

Fig. 2

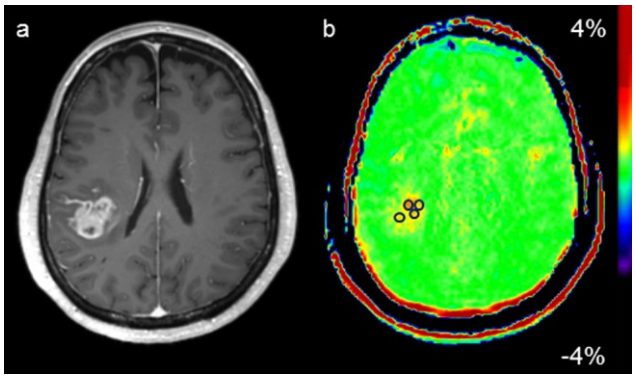

Fig. 3

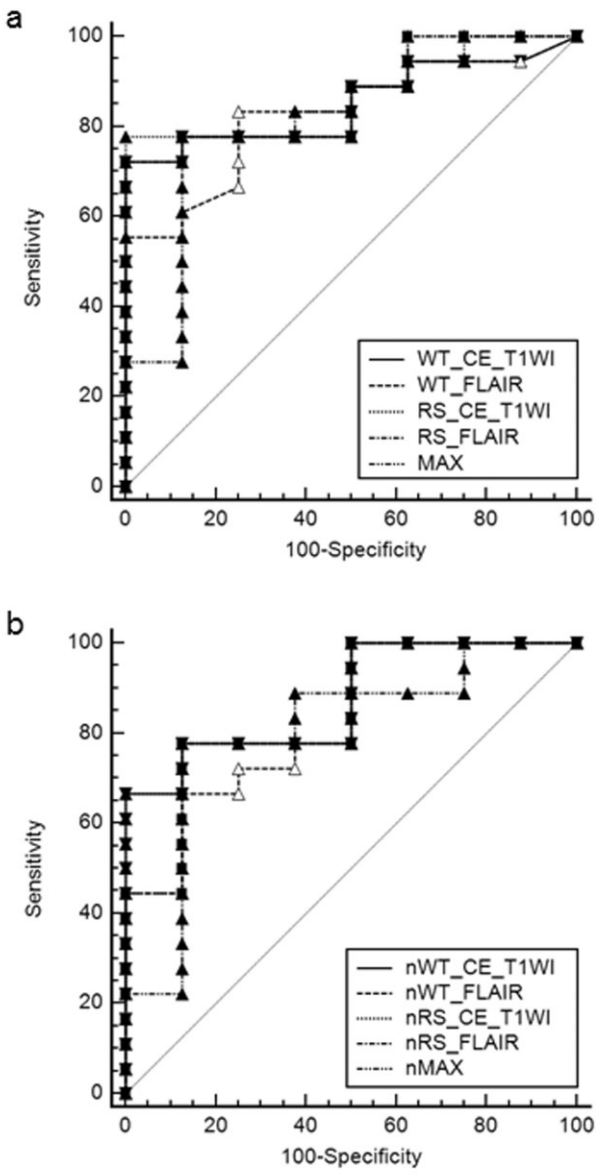
a
Sensitivity
100-Specificity
0
20
40
60
80
100
WT_CE_T1WI
WT_FLAIR
RS_CE_T1WI
RS_FLAIR
MAX
b
Sensitivity
100-Specificity
nWT_CE_T1WI
nWT_FLAIR
nRS_CE_T1WI
nRS_FLAIR
nMAX

Fig. 4

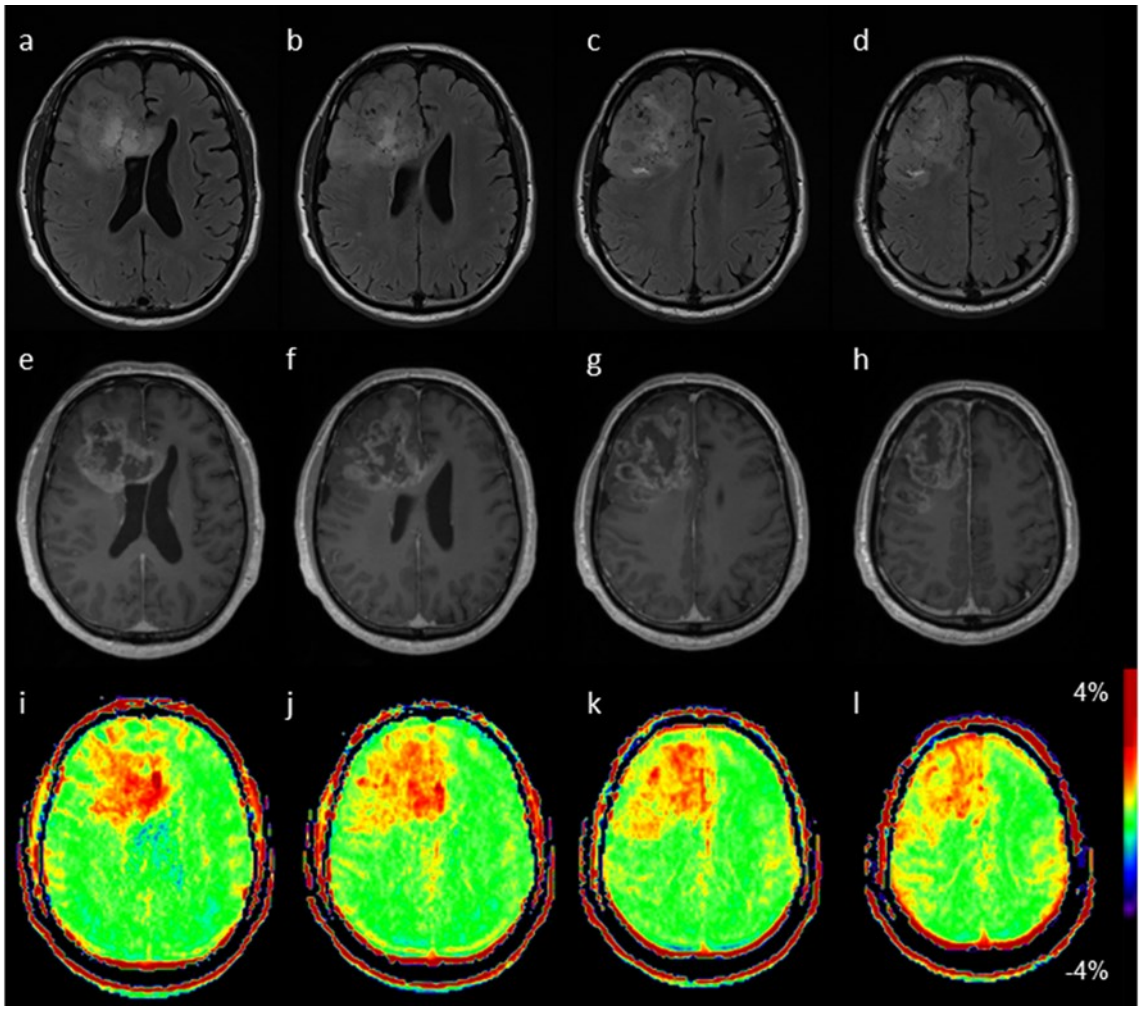

Table 1 Inter-observer agreement of APTasym measurements in glial tumors

Type of ROIs	ICC (95% CI)
WT-CE	0.99 (0.98 – 1.00)
WT-FLAIR	0.83 (0.67 – 0.93)
RS-CE	0.96 (0.91 – 0.98)
RS-FLAIR	0.88 (0.76 – 0.95)
MAX	0.96 (0.90 – 0.98)

ICC: Intra-class correlation coefficient, CE: Contrast-enhanced, FLAIR: Fluid-attenuated inversion-recovery, MAX: maximum, ROI: Regions-of-interest, RS: Representative-slice, WT: Whole tumor.

Table 2 Means and SD of APTasym values of different grades 2–4.

Grade	Number	APTasym					normalized APTasym				
		WT_CE_T1WI	WT_FLAIR	RS_CE_T1WI	RS_FLAIR	MAX	WT_CE_T1WI	WT_FLAIR	RS_CE_T1WI	RS_FLAIR	MAX
2	8	0.75±0.26[*1]	0.75±0.26[*2]	0.78±0.30[*1]	0.78±0.30[*1]	1.40±0.62[*2]	0.54±0.32[*1]	0.54±0.32[*2]	0.56±0.36[*1]	0.56±0.36[*2]	1.19±0.66[*2]
3	7	0.98±0.49[#1]	0.99±0.41	1.02±0.50[#1]	0.98±0.45[#2]	1.78±0.88	0.80±0.49[#2]	0.80±0.40	0.83±0.51[#2]	0.80±0.45	1.60±0.84
4	11	1.51±0.26	1.24±0.24	1.57±0.24	1.43±0.28	2.51±0.41	1.30±0.30	1.03±0.26	1.36±0.28	1.23±0.30	2.31±0.41

CE: Contrast-enhanced, FLAIR: Fluid-attenuated inversion-recovery, MAX: maximum, ROI: Region of interest, RS: Representative-slice, WT: Whole-tumor

T1WI: T1-weighted image.

[*1] $p<0.001$ between 2 and 4, [*2] $p<0.01$ between 2 and 4, [#1] $p<0.01$ between 3 and 4, and [#2] $p<0.05$ between 3 and 4.

Table 3 ROC analysis of APTasym values to differentiate high from low grades.

Number	APTasym					normalized APTasym				
	WT_CE_T1WI	WT_FLAIR	RS_CE_T1WI	RS_FLAIR	MAX	WT_CE_T1WI	WT_FLAIR	RS_CE_T1WI	RS_FLAIR	MAX
AUC	0.85	0.83	0.88	0.87	0.81	0.88	0.83	0.88	0.85	0.81
(95%CI)	(0.66–0.96)	(0.63–0.95)	(0.69–0.97)	(0.68–0.97)	(0.61–0.97)	(0.69–0.97)	(0.63–0.95)	(0.69–0.97)	(0.65–0.96)	(0.60–0.93)
Sensitivity	72.2	83.3	77.8	72	77.8	66.7	66.7	66.7	77.8	77.8
Specificity	100	75	100	100	87.5	100	87.5	100	87.5	87.5
Cut-off	1.11	0.89	1.21	1.21	1.63	0.97	0.87	1.07	0.90	1.44

AUC: Area under the curve, CE: Contrast-enhanced, FLAIR: Fluid-attenuated inversion-recovery, MAX: maximum ROI: Region-of-interest, RS: Representative-slice, WT: Whole-tumor, T1WI: T1-weighted images.